# *Role of seta angle and flexibility in the gecko adhesion mechanism*





| | |
|---|---|
| **Citation** | Hu, C., & Greaney, P. A. (2014). Role of seta angle and flexibility in the gecko adhesion mechanism. Journal of Applied Physics, 116(7), 074302. doi:10.1063/1.4892628 |
| **DOI** | 10.1063/1.4892628 |
| **Publisher** | American Institute of Physics Publishing |
| **Version** | Version of Record |
| **Terms of Use** | http://cdss.library.oregonstate.edu/sa-termsofuse |

# Role of seta angle and flexibility in the gecko adhesion mechanism

Congcong Hu and P. Alex Greaney[a)]
*School of Mechanical, Industrial, & Manufacturing Engineering, Oregon State University, Corvallis Oregon, 97331, USA*

(Received 20 March 2014; accepted 29 July 2014; published online 15 August 2014)

A model is developed to describe the reversible nature of gecko dry adhesion. The central aspect of this model is that the seta can be easily peeled away from the contacting surface by a small moment at the contact tip. It is shown that this contact condition is very sensitive, but can result in robust adhesion if individual setae are canted and highly flexible. In analogy to the "cone of friction," we consider the "adhesion region"—the domain of normal and tangential forces that maintain adhesion. Results demonstrate that this adhesion region is highly asymmetric enabling the gecko to adhere under a variety of loading conditions associated with scuttling horizontally, vertically, and inverted. Moreover, under each of these conditions, there is a low energy path to de-adhesion. In this model, obliquely canted seta (as possessed by geckos) rather than vertically aligned fibers (common in synthetic dry adhesive) provides the most robust adhesion. © *2014 AIP Publishing LLC*.
[http://dx.doi.org/10.1063/1.4892628]

## I. INTRODUCTION

Geckos are one of the most specialized climbers in nature having evolved a dry-adhesive that enables them to stick to almost all materials. Their ability to adhere comes from the van der Waals force from millions of branching hairs (setae) on the geckos' feet conforming to the contours of the surface.[1–3] These setae are just one part of a hierarchical adhesion system that maximizes surface contact area, even on fractally rough surfaces, and enables robust load sharing.[4–6,18] More importantly from the gecko's point of view, this is a *smart* adhesion system that provides highly reversible traction under a wide range of loading conditions—permitting geckos not just to stick but to also unstick rapidly, and enabling them to run at speeds of up to twenty body-lengths per second. Since the origin of the gecko's adhesion was unequivocally resolved in 2002 (Ref. 2) numerous groups have sought to create synthetic dry-adhesive tapes patterned with arrays of compliant microfibers or pillars that can replicate the phenomenon.[7–12] Development of these synthetic gecko adhesives has revealed a lot of the subtlety employed by real geckos. Recent studies have identified anisotropy of setae as a key feature necessary for smart or reversible adhesion.[11,13] Motivated by this, the latest generations of synthetic adhesives have explored a variety of strategies to create systematic anisotropy. These include presetting a seta at a canted angle,[9–11] using hybrid materials, and modifying the tip shape,[7,9] or vertical symmetrical microfibers.[8,12] These synthetic dry-adhesives have shown remarkable performance in certain desirable aspects; however, they still have a long way to go to match the performance of geckos themselves.

There are two major differences between synthetic dry-adhesives and gecko adhesion. First, many synthetic adhesives possess only one level of hierarchy (due to the complexity in the fabrication), while the gecko possesses an adhesion system with multiple levels of hierarchy spanning from its four feet, through toes, lamellae, to setae that branch three times at their tips. Second, many synthetic adhesives have fibers oriented vertically, while the gecko's setae are canted at an oblique angle. Computational models have been powerful for understanding the effect of these differences. Among these models, a discrete linear springs model by Bhushan explains the adhesion enhancements afforded by hierarchically branched setae.[14,15] Other models have represented individual seta as elastic beams in order to determine the optimal geometry for synthetic setae.[10–12,16] Both types of model have treated the seta tip as a point contact, and neither has provided a full explanation of smart de-adhesion. One mechanism for easy de-adhesion has been proposed by Takahashi who noted that setae have a finite width and would impart a moment at the contact surface[17] as shown in Fig. 1(a). This could be used by the gecko to pry rather than pull apart the contact between seta tips and an adhering surface. This is a compelling idea; however, no detailed model was built or analyzed until now.

In this work, we elucidate the central role that the combination of canted and flexible setae play both for adhesion and in Takahashi's mechanism for easy de-adhesion. We present two models of an adhering seta—the feature that distinguishes these from previous models is that the seta's contacting tip is able to support a moment. The first model is heuristic and demonstrates that flexibility of the seta is crucial for providing *robustness* of adhesion under dynamic loads while the moment enables easy de-adhesion. The second model is representative of a gecko seta and we use it to determine geometric parameters that would be optimal for the gecko.

## II. HEURISTIC MODEL

### A. Moment-supporting contact

The oblique seta angle has been proposed as the key factor for geckos' ability to easily unstick when they are

a)Author to whom correspondence should be addressed. Electronic mail: alex.greaney@oregonstate.edu; URL: http://research.engr.oregonstate.edu/greaney/

 

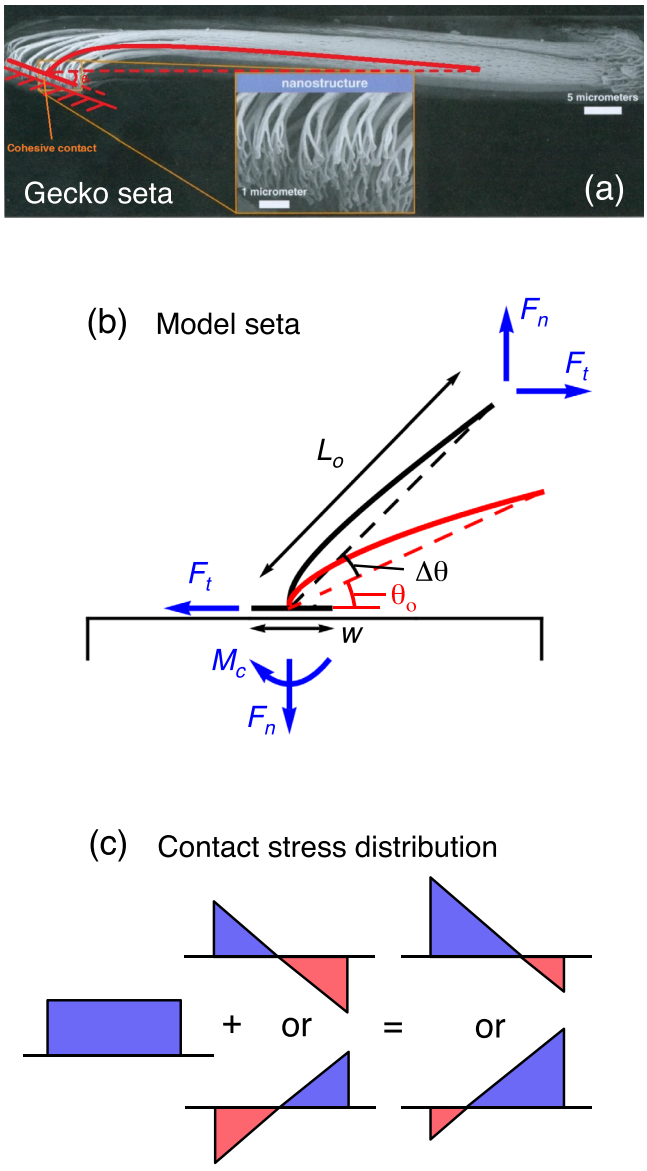


FIG. 1. (a) Scanning electron micrograph of a Tokay gecko (*Gekko gecko*) seta overlaid with a depiction of the model seta geometry considered in this work. The micrograph was taken by Kellar Autumn and originally published in Ref. 1 and is reproduced with the kind permission of the author. (b) Schematic of a seta contacting a surface. The red lines show the undeformed seta with the black lines showing a seta supporting normal and tangential forces $F_n$, and $F_t$. (c) Shows the normal stress distribution in the contacting pad due to a combination of the normal force $F_n$ and the moment $M_c$ at the contact. In this model, de-adhesion occurs when any portion of the stress distribution exceeds the tensile adhesion limit $\sigma_{ad}$.

walking or climbing. In order to explore the interplay of this canting angle with the soft compliance of a seta, a basic single seta model is constructed as is shown in Fig. 1(b). As is seen in Fig. 1(a), real setae have branched tips ending in an array of small contacts. In our model, we ignore the details of the branching and represent the array of contacts with a single planer contact pad that feels a non-uniform adhesive stress. The result is that the contact can support a small moment and that the contact moment can greatly affect the peak stress in the contact. We assume there to be a limiting stress, $\sigma_{ad}$ for adhesion, and if any part of the contacting area exceeds this limiting stress the seta de-bonds from the surface. Thus, as is shown in Fig. 1(c), the strength of the seta's adhesion is dependent not just on the normal load, but is also sensitive to the moment at the contact. This setup was first proposed by Takahashi[17]—it provides a mechanism to easily peel or pry off the contact when unsticking. The condition for adhesion is very sensitive to the moment $M_c$ at the contact requiring the horizontal and vertical loads on the seta to be carefully balanced during adhesion. In this work, we do not impose any limit to the tangential forces. There will clearly be a critical shear stress that causes the seta to slide; however this can be added without altering the mechanics of de-adhesion and so we omit it from the present calculations and consider its effect at the end.

The seta is taken to have a canting angle $\theta$, that is, the angle from the base of the seta to the contact ignoring the seta's curvature. The distal contact feels adhesion forces tangential, $F_t$ (positive towards the gecko), and normal, $F_n$, to the surface. As stated in Ref. 17, when $F_n/F_t = \tan(\theta)$, the moment imparted on the tip becomes zero and the normal stress is flat, distributed as show in the leftmost figure in Fig. 1(c). However, if the seta contact can support a small moment, then these two forces become decoupled and the moment at the contact, $M_c$, is given by

$$M_c = LF_t \sin(\theta) - LF_n \cos(\theta), \tag{1}$$

where $L$ is the distance from the contacting tip to the seta's root (indicated in Fig. 1(b)). The moment at the contact depends only on the forces at the seta's root and the position of the root. In this heuristic model, we assume the seta's root to be free to move and also to rotate. As can be seen in Fig. 1(c), the combination of a flat stress distribution generated by the normal force (left) with symmetric triangular stress distribution generated by the moment (middle) results in a non-uniform asymmetric stress distribution with the maximum normal stress on the edge given by

$$\sigma_{\max} b = \frac{6|M_c|}{w^2} + \frac{F_n}{w}, \tag{2}$$

where $w$ is the contacting width of the contact pad shown in Fig. 1(b), and $b$ is the thickness of the pad into the page. In this article, we will consider dimensionless versions of the forces $f$ and moment $m$ that we define as fractions of the pull of force: $f = \frac{F}{\sigma_{ad} wb}$ and $m = \frac{M}{L_o \sigma_{ad} wb}$, where $L_o$ is the undeformed length of the seta (in this model, we impose that $L = L_o$; but in the later model, this condition is relaxed). Using Eq. (2) with the adhesion criterion $\sigma_{ad} > \sigma_{\max}$ gives an upper and lower value for the dimensionless moment at the seta contact at detachment

$$1 = f_n \pm 6\lambda m_c, \tag{3}$$

where $\lambda = L_o/w$ is the seta aspect ratio. These equations bound the set of loading conditions, $f_n$ and $f_t$, for which the seta will remain stuck to the surface. If the seta remains rigid, then the dimensionless "adhesion region" is a slender oblique triangular wedge with width dictated by the aspect ratio $\lambda$. From Fig. 1(a), we estimate this aspect ratio to be in the range of 8–12 (we used 10 for the calculations reported

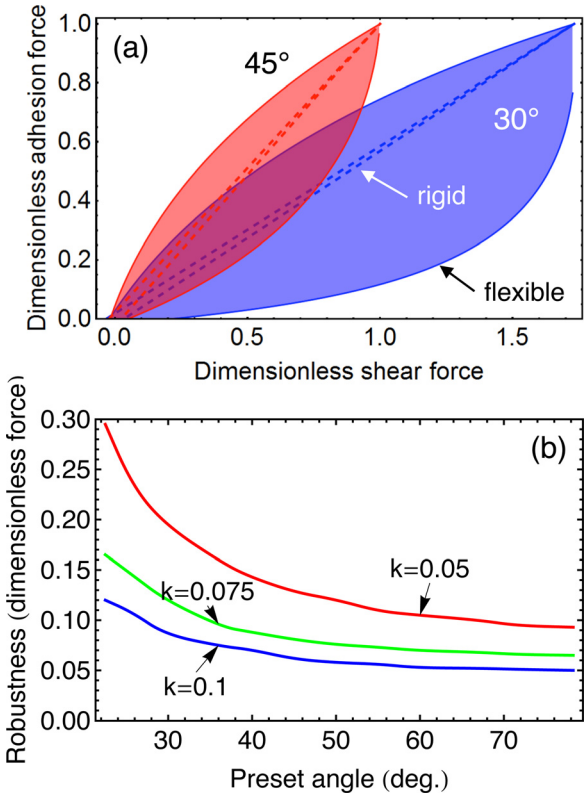


FIG. 2. (a) Dimensionless adhesion region of flexible and rigid seta computed with preset canting angles of $\theta_o = 45°$ (red) and $\theta_o = 30°$ (blue). In all cases, $\lambda = 10$. The flexible seta was computed with $k = 0.0375$. Allowing the seta to bend massively increases the adhesion region by deforming to reduce moments at the seta contact. (b) Plots the dimensionless robustness, which is quantified in units of dimensionless force (see text for details), for seta with varying dimensionless stiffness as a function of the preset canting angle.

here), which results in an very narrow adhesion region demarked by dashed lines in Fig. 2(a). Importantly, the adhesion region is asymmetric. To resist a large normal load, the gecko must supply a moment balancing tangential force inward (in a proximal direction). This asymmetry means that to easily de-adhere the gecko need only remove the tangential force. Clearly, the loads $f_n$ and $f_t$ on a seta will be very different depending on whether the gecko is running on a horizontal surface, climbing vertically or hanging inverted. Moreover, the $f_n/f_t$ ratio will differ dramatically as the gecko loads and unloads the seta, and will also differ between neighboring setae. Most surfaces are rough and so the contacts conditions vary from seta to seta. Performing dynamic motion while maintaining the majority of setae adhered to the surface will require a very broad set of adhesion conditions. The key to this is the ability of the seta to bend.

### B. Flexible seta

Under unbalanced loads, the seta will bend in the direction that reduces the lever arm of the dominant load (and increases the lever arm of the weaker force) and will thus buffer the effects of unbalanced moments from $f_n$ and $f_t$. We model the flexural behavior of the seta as a torsional spring with dimensionless stiffness, $k$, such that $k\Delta\theta = m_c$. The net dimensionless bending moment at the contact, $m_c$, is then a nonlinear function of the loading and is given by

$$m_c = f_t \sin(\theta_o + \Delta\theta) - f_n \cos(\theta_o + \Delta\theta), \quad (4)$$

where $\theta_o$ is the preset angle, i.e., the canting angle of the undeformed seta. The adhesion condition in Eq. (3) still holds. We compute the adhesion regions by solving Eqs. (3) and (4) numerically to find the $f_t$ and $\Delta\theta$ at the adhesion limit for a given value of $f_n$.

Figure 2(a) shows the adhesion regions for a flexible seta with preset angles of 45° and 30° (both with the same dimensionless stiffness $k = 0.0375$). Allowing the seta to bend greatly expands the adhesion region. While the adhesion region remains narrow for small $f_n$ and $f_t$, under large loads adhesion is robust to a wide range of load ratios $f_n/f_t$.

Marrying robustness of seta adhesion (a wide adhesion region) with easy de-attachment (asymmetric adhesion region) is essential for the gecko. In the gecko adhesion system, each seta does not work in isolation, but experiences a range of loads depending on the behavior of adjacent setae and its adhering to rough surfaces.

As a simple first metric of this, we consider the radius of loading space (i.e., the scatter in) $f_n$ and $f_t$ that the seta can tolerate and still remain stuck. This is quantified by finding the radius of the largest circle that can fit in the adhesion region (and thus, the radius of this circle is measured in units of dimensionless force). Figure 2(b) shows the plot of this radius as a function of canting angle for setae of different stiffnesses. While this metric has no rigorous theoretical foundation, it provides a completely objective metric that we can use to compare different seta geometries. It can be seen that orienting the seta with a more oblique angle greatly increases the width of the adhesion region, as does increasing seta flexibility.

In this model for dry adhesion, the resistance to tensile normal force results from an applied tangential force. It is instructive to make the comparison between the gecko adhesion and static friction as these are in many ways opposites (see Fig. 3). Static friction creates resistance to sliding forces as the result of a compressive normal force. The gecko's dry adhesion is able to resist a tensile normal force as a result of a tangential force. In order to generate adhesion, the gecko must press and slide its feet towards its body. This process enables setae to make intimate surface contact, however, we propose that this dragging also acts to balance moments that would otherwise peel away the setae contacts.

While our very simple heuristic model demonstrates that the combination of flexibility and oblique preset angle in moment supporting setae provides an advantage for adhesion, clearly there must be an optimal limit for each of these attributes. Setae that are too long or flexible will become matted and entangled with each other. If setae are too close to horizontal, the gecko must apply a huge tangential force to balance a moderate normal force. This will either result in setae sliding, or as biological motors require energy just to exert a *static* force, it will mean the gecko has to exert a lot of energy to adhere. All of these phenomena are excluded from our simple model but they allow us to identify the trade offs in the evolutionary optimization of the geckos' adhesion system. Setae must be stiff enough to creating a non-matting array with large area density. They must be moderately

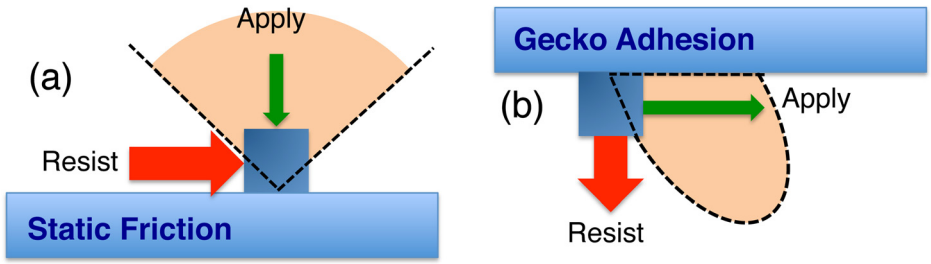


FIG. 3. Schematic contrasting geckos' dry adhesion with static friction. (a) Friction provides resistance to a shear force as a result of a compressive normal force. If the total force vector is anywhere inside the cone of friction, the interfaces will remain static. (b) Geckos resist a tensile normal load through the application of a shear force. The resulting force must lie inside the adhesion region for the joint to remain stuck. In contrast to friction, the adhesion region must be asymmetric to provide easy de-attachment.

canted to permit easy de-adhesion while only requiring moderate shear force from the gecko to hold a large normal force. Moreover, the gecko must be able to climb vertically as well as hang upside down—so a gecko's foot must be able to support a large tangential force with little normal force.

To explore methods to broaden the adhesion region in the simple model, we consider the effect of nonlinearity in the seta's flexibility. Real setae have a curved and branched structure and undergo large deformations. Thus it is reasonable to expect that the bending stiffness is nonlinear and asymmetric. To capture this, we replace the dimensionless linear bending stiffness with a nonlinear stiffness function

$$k_{nl} = k_1 + k_2\frac{\Delta\theta}{\theta_o} + k_3\left(\frac{\Delta\theta}{\theta_o}\right)^2, \tag{5}$$

where $k_2$ and $k_3$ are the first asymmetric and symmetric nonlinear stiffness terms. Positive $k_2$ stiffens the seta when it is bent down, and positive $k_3$ stiffens the seta under large deflections in either direction. The adhesion region of nonlinear setae is shown in Fig. 4. Very flexible setae provide a large and robust adhesion region with the limiting case of a perfectly flexible seta being equivalent to a point contact, with no easy path for de-adhesion. The design rational for non-linear stiffness is then to obtain a broad range of motion for the seta with little contact moment, but for the seta to stiffen outside of this range resulting in rapid detachment. Figure 4 demonstrates that only including a positive $k_3$ term can result in a large expansion of the adhesion region while still providing a route for easy unsticking.

## III. GECKO MODEL

### A. Gecko model setup

To further explore the mechanism for detachment, we consider the energy stored in the seta and the work of de-adhesion for various loading paths. The heuristic model is overly simplistic and includes no linear extension of the seta. This means that it would require no work to detach the seta if the force is applied along $\theta_o$. To correct this, we consider a second model that is more representative of a gecko seta and that permits us to examine work of de-adhesion. This model has two significant differences, first it assumes that the seta is extensible, and second that it supports a moment both at its tip, and at its root where it joins the gecko's foot, as shown in Fig. 5(a). We impose the boundary condition that as the seta flexes the contact pad must remain horizontal to stay bonded to the surface. This gives the condition that $\alpha_f + \alpha_m = 0$, where $\alpha_f$, and $\alpha_m$ are the rotation angle of the seta tip due to bending force, $(F_t L\sin(\theta) - F_n L\cos(\theta))$, and a moment $M_c$, respectively. We consider the seta as a curved beam with a varying moment of inertia and modulus, and we show that this geometry can be mapped to a simpler system of two torsional springs as shown in Fig. 5(b). In elastic beam theory, the bending angle from the base of a cantilevered beam to its tip $(\Delta\theta)$ scales linearly with the rotation angle at the free end $(\alpha)$ and can be expressed as $\frac{\alpha_f}{\Delta\theta_f} = \beta_f, \frac{\alpha_m}{\Delta\theta_m} = \beta_m$. Geometrically, the

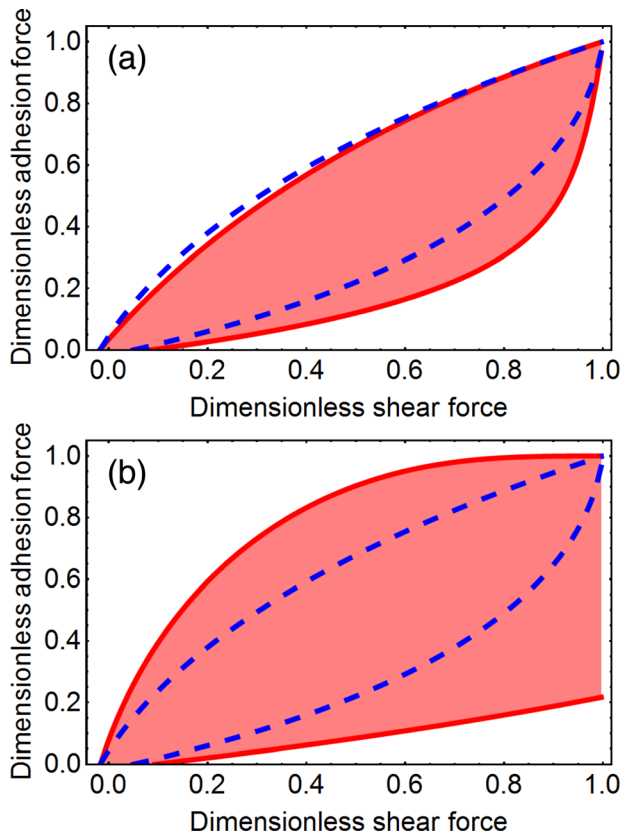


FIG. 4. Plot of the adhesion region for seta with nonlinear bending stiffness (red) overlid with the adhesion region for linear seta (blue). Plot (a) is computed with $k_1 = 0.0375$, $k_2 = 1$, and $k_3 = 1$. Plot (b) is computed with $k_1 = 0$, $k_2 = 0$, and $k_3 = 1$. In both (a) and (b), the blue overlaid curve is computed with $k_1 = 0.0375$, $k_2 = 0$, and $k_3 = 0$. In all cases, $\lambda = 10$ and $\theta_o = \frac{\pi}{4}$.

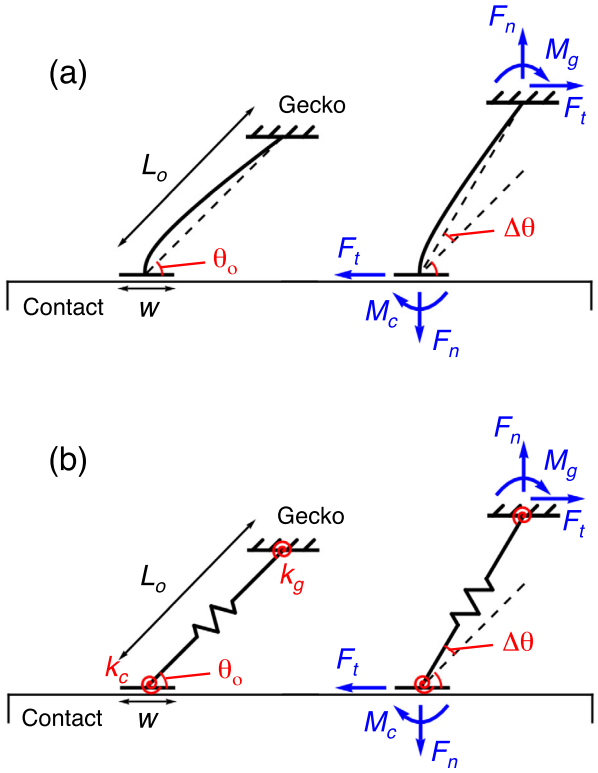


FIG. 5. (a) shows the schematic of a real gecko seta. The seta is cantilevered from its root and bends under the actions of bending forces ($F_t$ and $F_n$ give rise to bending force $F_t L\sin(\theta) - F_n L\cos(\theta)$) and moments ($M_c$) applied at its tip. While adhered to a surface, the contact pad must be rotated to remain parallel to the surface. (b) shows the beam like model of a seta from (a) mapped to a system of two torsional springs ($k_c$ and $k_g$). In both (a) and (b), the left hand figure shows the undeformed seta and the right hand side the seta supporting a load.

ratios $\beta$ must satisfy $\beta_m > \beta_f > 1$. (To provide some physical context for interpreting these geometric parameters, we note that $\beta_f$ and $\beta_m$ for a simple cantilever beam are 1.5 and 2, respectively.) The compatibility condition leads to the expression for the dimensionless moment at the contacting tip,

$$m_c = \frac{k_m\beta_f}{k_f\beta_m}\left(f_n\cos(\theta) - f_t\sin(\theta)\right), \tag{6}$$

where $k_f$ and $k_m$ are the dimensionless angular stiffness of the seta as a whole in response to a moment $m_g$ at the seta root imparted by either a bending force or a moment, respectively, applied at the seta tip. Note also that geometrically $k_f$ must be larger than $k_m$. From the balance of moments, this gives the ratio of contact to root moments

$$\frac{m_c}{m_g} = \frac{k_m\beta_f}{k_f\beta_m - k_m\beta_f}. \tag{7}$$

For a seta modeled as a curved beam, the values of $k_f$, $k_m$, $\beta_f$, and $\beta_m$ can be found from elementary mechanics using the unit load method. However, with the imposed boundary condition of zero net contact rotation, then we can find an equivalent two-torsional-spring system as depicted in Fig. 5(b) with $k_c = \frac{k_m\beta_f}{\beta_m-\beta_f}$ and $k_g = \frac{k_f\beta_m-k_m\beta_f}{\beta_m-\beta_f}$ that undergoes the same displacement and possesses the same moment ratio as the geometry-based model for a given loading condition. In this simpler system, $\Delta\theta = \frac{m_c}{k_c} = \frac{m_g}{k_g}$ and

$$\frac{m_c}{m_g} = \frac{k_c}{k_g} = \eta. \tag{8}$$

This means that the system response is described by an effective root stiffness $k_g$ and stiffness ratio $\eta$. Thus, rather than estimating $k_f$, $k_m$, $\beta_f$, and $\beta_m$ for seta shaped beams (which would contain much uncertainty), we determine the stiffness scale and ratio $\eta$ that is optimal for the gecko. We leave the problem of identifying beam geometries with the desired $\eta$ for later research.

Finally, a tensile stiffness $k_t$ is included to model elongation of the seta. The resulting contact moment is given by

$$m_c = (1+\varepsilon)(f_t\sin(\theta) - f_n\cos(\theta)), \tag{9}$$

with $\theta = \theta_o + \Delta\theta$, and the fractional elongation, $\varepsilon$, given by

$$\varepsilon = \frac{1}{k_t}\left(f_t\cos(\theta) + f_n\sin(\theta)\right). \tag{10}$$

As before, the limits for adhesion are given by Eq. (3).

### B. Gecko model: Results and discussion

The two-torsional-spring model has a qualitatively different adhesion region from the simple model as shown in Fig. 6. The two-spring model supports a much broader range of tangential forces under small normal force and thus provides more robust adhesion particularly during dynamic loading.

The plot in Fig. 6(c) shows the change in the adhesion region with an increase in tip stiffness $k_c$ (for constant tip/root stiffness ratio $\eta$), and the effect of reducing the tip/root stiffness ratio (for constant $k_c$). It is clear from these plots that the adhesion region expands with decreasing $\eta$, and decreasing $k_c$, i.e., setae that are flexible but stiffer at their root than at their tip. The density plots in Fig. 7 show the elastic energy stored in two setae as a function of loading conditions (the elastic energy is indicated by the colored shading with the thick black line marking the boundary of the adhesion region). Together these plots show that the tensile stiffness of the seta, $k_t$, plays a negligible role in determining the boundary of the adhesion region, but is important for the elastic energy, particularly under large tensile large loads. The curved shape of the gecko's setae makes them relatively soft in tension. Setae elongate by straightening under tensile loads and from the geometry of the seta in Fig. 1(a) we estimate that $k_t$ is 30–100 time larger than $k_c$. (This estimation was obtained by computing the extension and bending stiffness of a curved beam using the unit load method.)

The energy maps in Fig. 7 show that there is a good reason for having setae that are soft in tension. The elastic energy stored in the seta when it breaks free is lost and thus this energy is the work of detachment. The flexibility of a seta results in a large amount of deflection, and thus a large stored bending energy. The stored elastic energy is inversely proportional to the stiffness. If the tensile stiffness is too

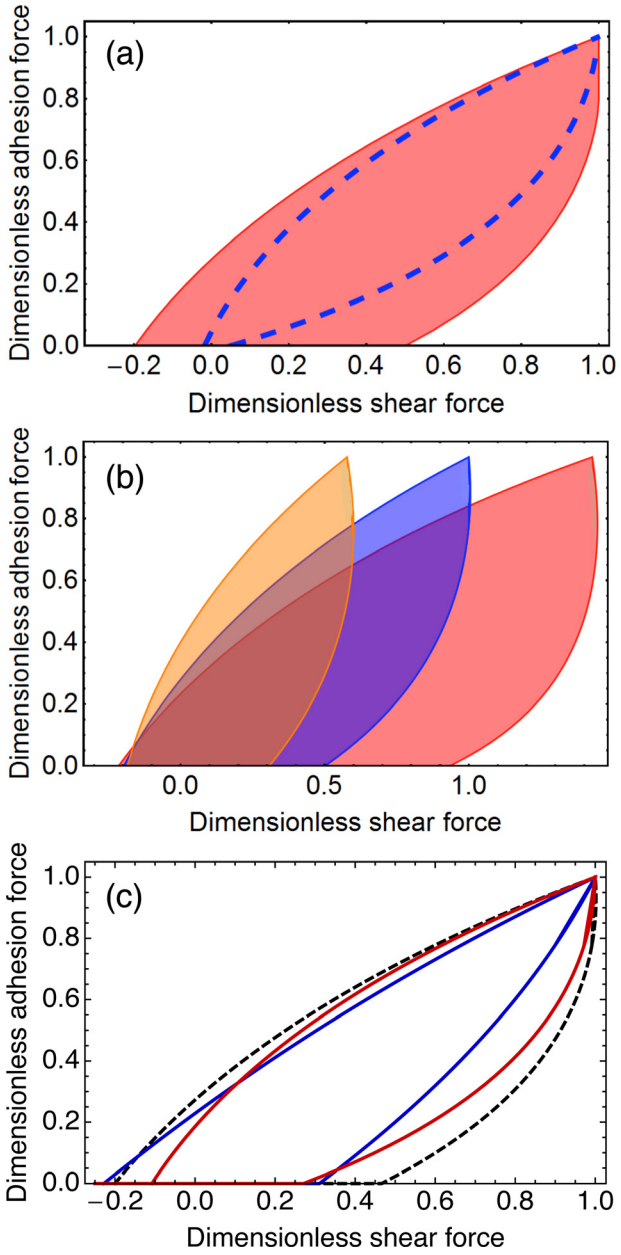


FIG. 6. Plots of the adhesion region of the two-torsional-spring model. (a) Comparison of the two-torsional-spring model (red) with the single-torsional-spring model (blue). (b) Plots of the adhesion region of the two-torsional-spring model of a seta with preset angles $\theta_o = 60^\circ$ (orange), $\theta_o = 45^\circ$ (blue), and $\theta_o = 35^\circ$ (red). (c) The change in adhesion region for varying $\eta$ and $k_c$. The dashed black line is computed with parameters were $\lambda = 10$, $\eta = 0.1$, $k_c = 0.0375$, and $k_t = 5$. The reducing $k_g$ by a factor of two produces the adhesion region plotted in red, and increasing $k_c$ by a factor of two results in the adhesion region plotted in blue.

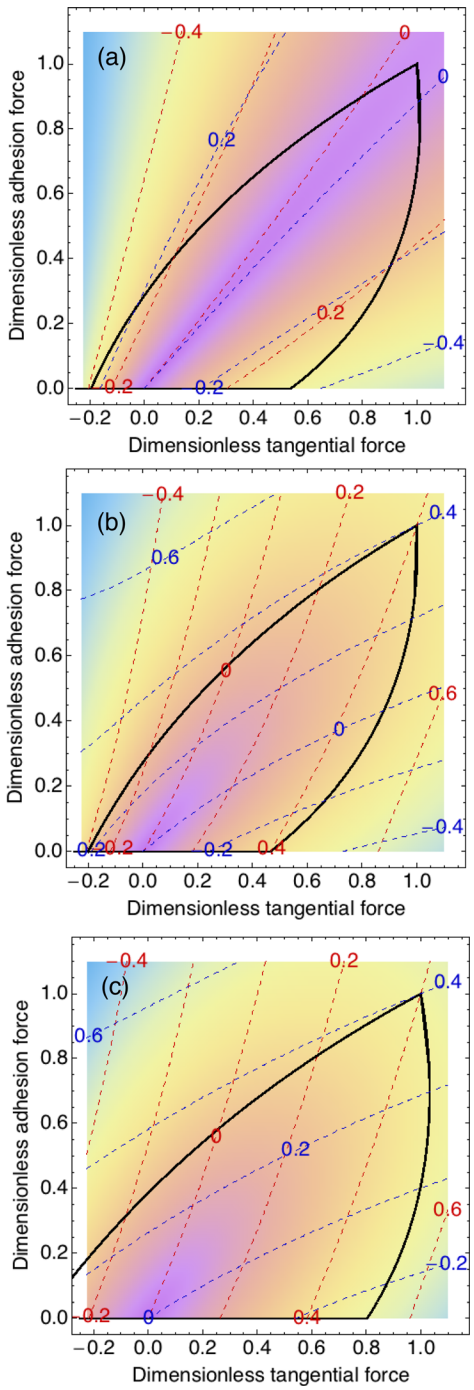


FIG. 7. Density maps of the stored elastic energy in a seta. Purple and pink indicates no or little stored energy and yellow and blue indicate moderate to large stored energy. The thick black line marks the boundary of the adhesion region and the red and blue dashed lines are contours of constant horizontal and vertical tip displacement, respectively. Plot (a) shows the energy map for a seta with large extensive stiffness, $k_t = 50$, and plot (b) shows the energy for a soft seta with $k_t = 5$. In both (a) and (b), the seta has canting angle $\theta_o = 45^\circ$ aspect ratio $\lambda = 10$, torsional stiffness ratio $\eta = 0.1$, and dimensionless tip stiffness $k_c = 0.0375$. It can be clearly seen that changing $k_t$ makes very little difference to the shape of the adhesion region, but dramatically alters the energy landscape. Plot (c) shows the energy for a seta that is soft in tension ($k_t = 5$) as in (b) but with a stiffer root so that the stiffness ratio $\eta = 0.05$. It can be seen that this increases the adhesion region but at the expense of a low energy detachment path. As can be gauged from the deflection contours on all plots, our choice of a soft root stiffness $k_g = 0.0375$ is sufficient permit the seta to bend a great deal but the angle of bending does not exceed $30^\circ$ anywhere in the adhesion region.

large relative to torsional stiffness (as in Fig. 7(a)), the lowest energy route for detachment is under a large $f_n$ and $f_t$. By reducing the axial stiffness to balance the torsional energy, one creates a tougher adhesive. Moreover, there is now an easy low energy pathway for detachment in which the stored elastic energy is recovered. This involves removing the tangential load $f_t$ (imparted by the gecko) before removing $f_n$. Plot (c) in Fig. 7 shows the energy map and adhesion region for a soft seta but with increased root stiffness $k_g$. It can be seen that stiffening the seta root enlarges the adhesion

region, but in doing so removes the low energy path for detachment and thus would not be optimal for the gecko. From the maps in Fig. 7, we see that there must be an optimal balance of $k_c$, $k_g$, and $k_t$ that give the potential for large stored energy (and thus tough adhesion), but tradeoff a large adhesion region (and thus robust adhesion) with a low energy de-adhesion path (and thus efficiency for the gecko).

Going beyond calculating the work of de-adhesion, we can consider the work done by $f_t$ and $f_n$ along different pathways to de-adhesion. The dashed contour lines on Figs. 7(a)–7(c) indicate lines of constant horizontal (red) vertical (blue) displacement of the seta root. Thus for loading or unloading along any of the red contours, $f_t$ does no work and $f_n$ performs no work during loading paths that follow the blue contours. We now consider three loading scenarios and examine potential unloading paths for each.

Case 1: Large $f_n$ and moderate $f_t$. This loading condition arises when the gecko is walking upside down sticking to inverted horizontal surfaces. The gecko must supply force $f_t$ to stick but gravity supplies $f_n$. Under these conditions, an adhered seta has a large quantity of stored energy. This energy is easily recovered to $f_t$ by an unloading path that follows a blue contour. By recovering the energy to work along $f_t$, the energy is returned to the gecko.

Case 2: Low $f_n$ and $f_t$. This loading condition arises when the gecko is walking normally on flat surfaces. The gecko requires a low energy, low force, detachment path. This is achieved by a small negative (distal) $f_t$ and $f_n$. The minimum force for detachment can be reduced by increasing the tip/root stiffness ratio ($\eta$) to increase the anisotropy in the adhesion region at $f_n = 0$. By having canted setae, the default stickiness of the gecko's foot is relatively low. Strong adhesion must be activated by a tangential force.

Case 3: Small or moderate $f_n$ and large $f_t$. This loading condition arises when the gecko is climbing vertical surfaces. The gecko must be able to resist large $f_t$ from gravity with relatively little moment balancing $f_n$. Under these conditions, the gecko has an easy path to de-adhesion by first unloading $f_n$ and then following the path in case 2. To be able to stick while climbing vertically, the adhesive needs to provide a large static friction force with a small tensile load. This necessitates an adhesion region that extends along the $f_t$ axis as seen in Figs. 7(a)–7(c).

The energy maps in Fig. 7 provide some insight into why the gecko's adhesion system is so successful. When moving around, the gecko wants to expend as little energy as possible and so the gecko needs a pathway in which it can unstick without expending energy. However, when jumping, catching itself, or changing directions quickly to avoid predation, the gecko's adhesion system has to absorb a great deal of energy. Moreover, the gecko's adhesion system needs to be able to provide these different functions across a wide range of orientations—that is, with gravity pointing in different directions. The map in Fig. 7(b) shows that a seta can perform all of these functions: creating tough adhesion under certain load directions but with unloading paths for de-adhesion that can return most of the stored elastic energy to the gecko. The red and blue contours show that different unloading paths can be used to return energy as work along either $f_n$ or $f_t$. This is significant as depending on the gecko's orientation, either $f_n$ or $f_t$ could be supplied by the gecko with the other force component coming from gravity.

The balance of flexibility and extensibility of the seta enables this energy absorption and return to happen at the seta level producing a tough joint with a large work of de-adhesion. Although the returned elastic energy will not return to chemical energy in the gecko's muscles, it is returned to elastic energy in the gecko's muscular system and so we consider it "recovered." It is beyond the scope of this article to examine the biodynamics and physiology of gecko locomotion but we note that there are other animals that are well known to recovered elastic energy in locomotion—most notably the jumping kangaroo. The seta is only one part in the gecko's hierarchical system of adhesion that spans from legs through toes and lamellae to setae and spatulae. Assuming that evolution has created the seta not in isolation but as part of a highly energy efficient system, our work raises the interesting question about how the compliance of the setae is matched to that of the lamellae and the rest of the gecko's physiology in order to utilize energy return. It is interesting that the combined area of setae over a gecko's four feet is sufficient to support approximately 50 times its body weight. We speculate that this limiting force is correlated with some other system level behavior such as the number of Gs other parts of the gecko can sustain, the maximum power output from the geckos muscles, or the natural resonant frequency of the gecko hanging from its legs.

## IV. CONCLUSIONS

We have developed two models that explore the mechanism for easy detachment in gecko adhesion. This mechanism is based on the interplay of two processes: moments at the seta contact pry off the seta providing low energy de-adhesion; bending by a flexible seta screens the buildup moments at the seta contact and so provides a broad range of loading conditions under which the seta will remain stuck. Central to the interplay of these two processes is that the seta is at an oblique angle. The oblique canting angle has the effect of making the seta in the permanently *unsticky* configuration with adhesion only activated by a moment balancing tangential force supplied by the gecko. Moreover, we show with this simple model that robustness of adhesion can be greatly increased while still possessing easy detachment if the seta has a nonlinear bending stiffness.

Our second, more realistic model of the gecko seta shows that low $k_c$ and low $\eta$ can produce a large robust adhesion region with a low energy path for unsticking from a variety of different loading conditions that the gecko might experience during walking, climbing, and hanging.

Together the findings from these two models have important ramifications for the development of synthetic dry adhesives. They show that to optimize adhesion synthetic seta must be designed holistically in a way that matches the geometry of the tip with the flexibility and canting angle of the rest of the fiber. Our models show that curved setae increase the toughness of the adhesive, and that creating

synthetic setae with nonlinear flexibility could greatly increase robustness of the adhesive.

## ACKNOWLEDGMENTS

The authors thank Dr. David Hackleman for insightful and thought provoking discussion. This work benefited from the Extreme Science and Engineering Discovery Environment (XSEDE), which is supported by National Science Foundation Grant Number OCI-1053575.

[1]K. Autumn, Am. Sci. **94**, 124 (2006).
[2]K. Autumn and A. M. Peattie, Integr. Comparative Biol. **42**, 1081 (2002).
[3]K. Autumn, M. Sitti, Y. A. Liang, A. M. Peattie, W. R. Hansen, S. Sponberg, T. W. Kenny, R. Fearing, J. N. Israelachvili, and R. J. Full, Proc. Natl. Acad. Sci. U.S.A. **99**, 12252 (2002).
[4]N. M. Pugno and E. Lepore, "Bio(nano)materials with structure-property relationship International Symposium on Bionanomaterials," Biosystems **94**, 218 (2008).
[5]B. Persson, Surf. Sci. Rep. **61**, 201 (2006).
[6]K. Autumn and N. Gravish, Philos. Trans. R. Soc. A **366**, 1575 (2008).
[7]J. Tamelier, S. Chary, and K. L. Turner, Langmuir **28**, 8746 (2012).
[8]L. Ge, S. Sethi, L. Ci, P. M. Ajayan, and A. Dhinojwala, Proc. Natl. Acad. Sci. U.S.A. **104**, 10792 (2007).
[9]H. E. Jeong, J.-K. Lee, H. N. Kim, S. H. Moon, and K. Y. Suh, Proc. Natl. Acad. Sci. U.S.A. **106**, 5639 (2009).
[10]B. Aksak, M. P. Murphy, and M. Sitti, Langmuir **23**, 3322 (2007).
[11]J. Lee, R. S. Fearing, and K. Komvopoulos, Appl. Phys. Lett. **93**, 191910 (2008).
[12]T.-i. Kim, H. E. Jeong, K. Y. Suh, and H. H. Lee, Adv. Mater. **21**, 2276 (2009).
[13]N. Gravish, M. Wilkinson, and K. Autumn, J. R. Soc. Interface **5**, 339 (2008).
[14]B. Bhushan, A. G. Peressadko, and T.-W. Kim, J. Adhesion Sci. Technol. **20**, 1475 (2006).
[15]T. W. Kim and B. Bhushan, J. Adhesion Sci. Technol. **21**, 1 (2007).
[16]M. Sitti and R. S. Fearing, J. Adhesion Sci. Technol. **17**, 1055 (2003).
[17]K. Takahashi, J. O. L. Berengueres, and S. Saito, Int. J. Adhesion Adhesives **26**, 639 (2006).
[18]N. Gravish, M. Wilkinson, and K. Autumn, J. R. Soc. Interface **5**(20), 339 (2008).